

Multicellularity of delicate topological insulators

Aleksandra Nelson,^{1,*} Titus Neupert,¹ Tomáš Bzdušek,^{2,1} and A. Alexandradinata^{3,†}

¹*Department of Physics, University of Zurich, Winterthurerstrasse 190, 8057 Zurich, Switzerland*

²*Condensed Matter Theory Group, Paul Scherrer Institute, 5232 Villigen PSI, Switzerland*

³*Department of Physics, University of Illinois at Urbana-Champaign, Urbana, Illinois 61801-2918, USA*
(Dated: March 6, 2022)

Being Wannierizable is not the end of the story for topological insulators. We introduce a family of topological insulators that would be considered trivial in the paradigm set by the tenfold way, topological quantum chemistry, and the method of symmetry-based indicators. Despite having a symmetric, exponentially-localized Wannier representation, each Wannier function cannot be completely localized to a single primitive unit cell in the bulk. Such *multicellular topology* is shown to be neither stable, nor fragile, but *delicate*, i.e., the topology can be nullified by adding trivial bands to either valence or conduction band.

Introduction.— Two themes have indelibly shaped the paradigm of topological insulators, and couched how topological properties are discussed, modelled, and measured. The first is the notion of stability of topological insulators, and the second involves the various obstructions that exist in forming a real-space Wannier representation of the valence band [1–8]. This work describes an extension and fine-graining of both themes, and in so doing introduces a novel family of topological insulators that would be considered unstable and unobstructed according to the presently-held paradigm.

The strongest form of stability is the notion of stable equivalence introduced from K -theory [8–12], where the topological property (be it a bulk invariant or surface state) of a valence band is immune to addition of trivial bands. The intermediate notion of fragility means that the topological property can be nullified by adding trivial bands to the valence band, but not to the conduction band [13–18]. A distinct notion that we introduce here is *delicate topology*, where the topological property can be nullified by adding trivial bands to either valence or conduction band. For symmetry-protected delicate topology, nullification occurs only by adding trivial bands of certain symmetry representations, while for non-symmetry-protected delicate topology, any trivial band will do.

Many authors have proposed a useful definition of a trivial band is its possession of an exponentially-localized Wannier representation respecting the crystallographic spacetime symmetries of the solid in question [11, 12, 18–22]. By this definition, all stably-equivalent and fragile topological insulators present an obstruction to such a Wannier representation. It has been further argued through equivariant vector bundle theory that such Wannier obstructions represent a robust property of a valence subspace summed with an *arbitrary* conduction subspace [18], and therefore such obstruction cannot exist for delicate topological insulators. Here, we introduce a distinct class of obstructions that prevents a Wannier function from being completely localized to a single, primitive unit cell – we call this *multicellular topology*. Conversely, we adopt a distinct notion of triviality, namely that symmetry-respecting Wannier functions exist and can be confined to a single cell by

a continuous, adiabatic deformation – *unicellularity*.

The notions of delicate and multicellular topology are distinct and a priori need not come together in any specific realization of a topological insulator. This work aims to open the debate by presenting a concrete family of tight-binding models which simultaneously manifests both types of topology, and sets the stage for future realizations and discoveries.

Returning Thouless pump.— We begin by introducing a class of tight-binding models in three spatial dimensions, which exhibit both symmetry-protected delicacy and multicellularity. The relevant symmetry is an n -fold rotation symmetry C_n about the z axis. The tight-binding Hilbert space is given by an orthonormal set of Wannier functions $\{\varphi_{j,R}\}_{R \in \text{BL}, j=1 \dots C+V}$ over the Bravais lattice BL, which satisfy the following *uniaxial symmetry* condition, i.e., that all independent Wannier functions (numbered $C+V$) within a representative, primitive unit cell are centered on the same rotational axis, and individually form one-dimensional representations of C_n . (This simplifying assumption holds only for a subclass of multicellular topological insulators studied here.) This allows to decompose the Hilbert space as $\mathcal{H}[\varphi] = \bigoplus_{\ell=0}^{n-1} \mathcal{H}_\ell[\varphi]$, where the summands are distinguished by the n possible angular momenta ℓ .

We further assume that the valence (resp. conduction) bands are spanned by a set of exponentially-localized Wannier functions $\{W_{j,R}^v\}_{R \in \text{BL}, j=1 \dots V}$ (resp. $\{W_{j,R}^c\}_{R \in \text{BL}, j=1 \dots C}$). Though generally distinct from the basis functions $\{\varphi_{j,R}\}$, we demand that $\{W_{j,R}^{c/v}\}$ also satisfy the uniaxial symmetry condition, and additionally satisfy the *mutually-exclusive* condition – that any representation appearing in the valence subspace cannot appear in the conduction subspace (e.g., for $n=4$, if the valence-band Wannier functions transform in either the $\ell=0$ or $\ell=1$ representation, then the conduction-band Wannier functions can only have $\ell \in \{2, 3\}$). More generally, the Hilbert subspace of the valence band is decomposable as $\mathcal{H}[W^v] = \bigoplus_{\ell_v} \mathcal{H}_{\ell_v}[W^v]$, and likewise for the conduction band $\mathcal{H}[W^c] = \bigoplus_{\ell_c} \mathcal{H}_{\ell_c}[W^c]$, where the angular momentum values $\ell_{v(c)}$ for the valence (conduction) bands are disjoint: $\ell_v \cap \ell_c = \emptyset$.

The uniaxial symmetry condition on exponentially-localized Wannier functions implies that both conduction and valence bands are band representations [23, 24], making the system trivial from the viewpoint of topological quantum chemistry [19] and the method of symmetry-based indica-

* anelson@physik.uzh.ch

† alexan7@illinois.edu

tors [21]. A band representation also precludes a nontrivial first Chern class [18, 22], making the model trivial in the tenfold way [9, 25, 26]. Nevertheless, we find that the mutually exclusive condition allows for a type of symmetry-protected multicellularity, where the Wannier functions necessarily extend – *beyond one unit cell* – in the direction of the rotation axis.

The multicellularity manifests in the discrete spectrum of the projected position operator $P\hat{z}P$ [27, 28], with P projecting to the bulk valence band. Since translations perpendicular to the rotation axis are symmetries of $P\hat{z}P$, each eigenvalue forms a band over the two-dimensional (2D) *reduced Brillouin zone*, $\text{rBZ} \ni \mathbf{k}_\perp = (k_x, k_y)$. Under translation along the rotation axis by a lattice period (set to one), $P\hat{z}P \rightarrow P(\hat{z}+1)P$, hence each eigenvalue belongs to an infinite Wannier-Stark ladder [29], and the full spectrum comprises \mathcal{V} such ladders which are typically non-degenerate at generic \mathbf{k}_\perp [7]. We pick one representative eigenvalue from each ladder, and define their sum to be the polarization $\mathcal{P}(\mathbf{k}_\perp)$; \mathcal{P} is well-defined modulo integer, in accordance with the geometric theory of polarization [30, 31].

Since distinct rotational representations cannot mix at C_n -invariant points of the rBZ satisfying $\mathbf{k}'_\perp \equiv C_n \mathbf{k}_\perp$, the polarization can be decomposed into a sum of polarizations in each angular-momentum sector: $\mathcal{P}(\mathbf{k}'_\perp) = \sum_{\ell_v} \mathcal{P}_{\ell_v}(\mathbf{k}'_\perp)$. This non-mixing, combined with the mutually-exclusive condition, implies an identity between symmetry-decomposed Hilbert spaces $\mathcal{H}_{\ell_v}[W^\nu]|_{\mathbf{k}_\perp} = \mathcal{H}_{\ell_v}[\varphi]|_{\mathbf{k}_\perp}$ when restricted to any C_n -invariant wavevector. It follows that the polarization $\mathcal{P}_{\ell_v}(\mathbf{k}'_\perp)$ equals, modulo integer, to the polarization of the basis Wannier functions φ in the spin sector ℓ_v ; the latter quantity is \mathbf{k}'_\perp -independent because any tight-binding basis function has support only on a single lattice site. Therefore, modulo integer, $\mathcal{P}_{\ell_v}(\mathbf{k}'_\perp)$ is independent of \mathbf{k}'_\perp , and hence also $\mathcal{P}(\mathbf{k}'_\perp)$. If $\mathcal{P}(\mathbf{k}_\perp)$ is continuously defined over rBZ with multiple C_n -invariant points, the difference $\Delta\mathcal{P}_{\mathbf{k}'_\perp, \mathbf{k}''_\perp} := \mathcal{P}(\mathbf{k}'_\perp) - \mathcal{P}(\mathbf{k}''_\perp)$ between any pair of these points is quantized to integers. $\Delta\mathcal{P}_{\mathbf{k}'_\perp, \mathbf{k}''_\perp} = \mu$ implies a Thouless pump [32] of μ electron

charges over one half-period of the rBZ (connecting \mathbf{k}'_\perp and \mathbf{k}''_\perp); the triviality of the first Chern class ensures that this charge is reversed in the second half-period. Such a *returning Thouless pump* (RTP) guarantees that: (i) the Hamiltonian cannot be adiabatically and continuously deformed to be \mathbf{k} -independent (having no hopping elements in real space), and (ii) at least one Wannier function must extend over *multiple unit cells* in the direction of the rotation axis.

Minimal model.— To exemplify a non-trivial RTP, we consider a two-band, tight-binding model with six-fold (C_6) rotational symmetry. On each site of a triangular lattice, we situate an s and a $p_+ = p_x + ip_y$ (spinless) orbital, which transform under C_6 with angular momenta $\ell=0$ and $\ell=1$, respectively. In the momentum representation, the Hamiltonian has the form

$$H(\mathbf{k}) = [z^\dagger(\mathbf{k})\boldsymbol{\sigma}z(\mathbf{k})] \cdot \boldsymbol{\sigma}, \quad z(\mathbf{k}) = (z_1, z_2)^T$$

$$z_1(\mathbf{k}) = \sum_{a=1}^6 e^{-ina/3} \exp\{it(a) \cdot \mathbf{k}_\perp\},$$

$$z_2(\mathbf{k}) = \sin k_z + i \left(\sum_{a=1}^6 \exp\{it(a) \cdot \mathbf{k}_\perp\} + 4 \cos k_z + m \right),$$
(1)

with $t(a) = (\cos(\pi a/3), \sin(\pi a/3))$ and $\boldsymbol{\sigma}$ the vector of Pauli matrices; the pseudospin $\langle\sigma_z\rangle=1$ (resp. -1) corresponds to the $\ell=0$ (resp. $\ell=1$) orbital. The model has been designed such that the mutually-exclusive condition is satisfied for any $m \in \mathbb{R}$, with the valence (resp. conduction) band spanned by s -type (resp. p_+ -type) Wannier functions. Applying our previous argument for $n=2$ and $n=3$, we find that the polarization at all C_2 -invariant points (Γ, M, M', M'') and C_3 -invariant points (Γ, K, K') in the rBZ [cf. Fig. 1(a)] are identical modulo integer. The six-fold symmetry implies there are only two independent polarization differences $\Delta\mathcal{P}_{\text{K}\Gamma}$ and $\Delta\mathcal{P}_{\text{M}\Gamma}$.

For large $|m|$, the Hamiltonian reduces to a \mathbf{k} -independent form $H(\mathbf{k}) \approx -m^2 \sigma_z$ without any hopping, implying that the s -type valence (and also the p_+ -type conduction) band is spanned by Wannier functions which are individually localized to a single unit cell; recall that unicellularity is our definition of triviality. This is consistent with a trivial RTP for representative values $m=-11$ and $m=8$ [as illustrated by the blue resp. brown line in Fig. 1(c)], meaning $\mathcal{P}(\mathbf{k}_\perp)$ is continuously deformable to a flat sheet. Increasing m from -11 to -10 , the bulk gap closes at the Brillouin-zone center; a small-momentum expansion gives an effective Hamiltonian of the form in Eq. (1) with $z_1 = 3(k_y + ik_x)$ and $z_2 = k_z + i(10+m)$, resulting in a quadratic energy-momentum dispersion (for both conduction and valence bands) in all three directions. The form of z identifies the band touching point as a *dipole* source of Berry curvature [33] with dipole moment parallel to the rotation-invariant \mathbf{k} -line. Such a dipole marks the critical point for a valence-to-conduction transfer of a 2π quantum of the Berry-Zak phase (ϕ_Z) – defined for the parallel transport of Bloch functions along said \mathbf{k} -line. Since $\phi_Z/2\pi \equiv \mathcal{P}(\Gamma)$ according to the geometric theory of polarization [30, 31], there is correspondingly a discontinuous, unit-decrease of $\Delta\mathcal{P}_{\text{M}\Gamma}$ and $\Delta\mathcal{P}_{\text{K}\Gamma}$ when the gap reopens for $m \gtrsim -10$, as illustrated by the orange line in Fig. 1(c). Note the gap closing is not accompanied by an inversion of bulk symmetry representations, hence

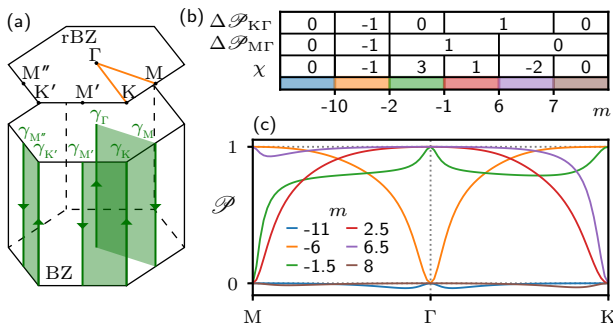


Figure 1. Bottom of panel (a): Brillouin zone of the C_6 -symmetric model (1) with rotation-invariant lines $\{\gamma_{\mathbf{k}'_\perp}\}$ colored green. Top of (a): the reduced Brillouin zone. (b) The polarization differences and the Hopf invariant are given as a function of $m \in \mathbb{R}$ for the model in Eq. (1), with colors distinguishing between distinct topological phases. (c) For each phase the polarization (along $\text{M}\Gamma\text{K}$) is plotted (with the same color) for a representative parameter value.

the valence (and conduction) band retains an exponentially-localized, uniaxially-symmetric Wannier representation; yet the nontrivial RTP guarantees that the same Wannier functions are multicellular. Further gap closings (at $m=-2, -1, 6, 7$) can be understood through Berry dipoles at other high-symmetry wavevectors, with the resultant phase diagram and RTP's summarized in Fig. 1(b,c).

Stability of RTP.— Equation (1) represents a minimal model of an RTP with the smallest matrix dimension for the Hamiltonian $H(\mathbf{k})$. Models of arbitrarily large matrix dimensions can be constructed from our minimal model by adding unicellular bands (in either conduction or valence subspace) that maintain the mutually-exclusive condition – this guarantees that the integer-valued quantization of $\Delta\mathcal{P}_{\text{M}\Gamma}$ and $\Delta\mathcal{P}_{\text{K}\Gamma}$ is preserved, hence also the RTP. In contrast (as numerically verified in the Supplemental Material [34]), the quantization is lost upon addition of unicellular bands that nullify the mutually-exclusive condition. Because the RTP can be nullified by addition of unicellular conduction bands of a certain symmetry representation (but not of other representations), we see that the RTP exemplifies a symmetry-protected delicate invariant.

Multicellularity with only translational symmetry.— Which of our conclusions survive when rotational symmetry is relaxed? While the RTP is no longer a robust feature, we show that multicellularity persists – at least for the minimal model and any continuous deformation thereof that preserves the bulk energy gap and the bulk *translational* symmetry; any other symmetry can be relaxed. We appeal here to a special feature of Pauli-matrix Hamiltonians with a spectral gap at each \mathbf{k} ; namely, that even with a trivial first Chern class, $H(\mathbf{k})=-\mathbf{h}(\mathbf{k})\cdot\boldsymbol{\sigma}$ has an integer-valued classification given by the Hopf invariant χ [35–37]. This invariant is inspired by the Hopf map in differential topology [38], and can be expressed as a Brillouin-zone (BZ) integral of the Abelian Chern-Simons three-form [37, 39]

$$\chi = -\frac{1}{4\pi^2} \int_{\text{BZ}} \mathbf{A} \cdot (\nabla \times \mathbf{A}) \, d^3k, \quad (2)$$

with $\mathbf{A}(\mathbf{k})=\langle u|i\nabla_{\mathbf{k}}u\rangle$ the Berry connection of an energy-nondegenerate band [40]. Since χ is only integer-quantized for Pauli-matrix Hamiltonians, it is manifestly a delicate topological invariant distinct from the RTP.

That our minimal model for $m\geq-10$ has $\chi=-1$ can be deduced from the known fact that a single Berry dipole intermediates a unit change in χ [33]. That $\chi\neq 0$ implies multicellularity is now proven by contradiction. Assume that a representative Wannier function for the valence band is localizable to one unit cell, i.e., $W_{\mathbf{R}}^v=\delta_{\mathbf{R},0}\kappa_v$, with κ_v a pseudo-spinor wave function that corresponds to a single point on the Bloch sphere S^2 . The Fourier transform of $W_{\mathbf{R}}^v$ is then simply $u_v(\mathbf{k})=\kappa_v$ that is \mathbf{k} -independent. It is an eigenvector of a Hamiltonian that represents the trivial, constant map from the BZ to S^2 , in contradiction with the assumed non-trivial Hopf invariant.

Hopf-RTP correspondence.— We have thus shown that *both* the Hopf invariant and RTP imply multicellularity, yet we have not shown that a nontrivial Hopf invariant implies a nontrivial RTP (or vice versa), when C_6 symmetry is retained. Such an implication is given, modulo six, by the following

Hopf-RTP correspondence:

$$\chi \equiv_6 3\Delta\mathcal{P}_{\text{M}\Gamma} - 2\Delta\mathcal{P}_{\text{K}\Gamma}, \quad (3)$$

where $a \equiv_6 b$ means “equal (mod 6)”. The correspondence holds for any C_6 -symmetric, Pauli-matrix Hamiltonian with trivial first Chern class and with the mutually-exclusive symmetry representations $\ell_v=0$ and $\ell_c=1$. (More general correspondences for any $\{C_n, \ell_v, \ell_c\}$ will be presented in a follow-up work.)

To prove Eq. (3), observe that the right-hand side is equivalently expressed as

$$3\Delta\mathcal{P}_{\text{M}\Gamma} - 2\Delta\mathcal{P}_{\text{K}\Gamma} = \Delta\mathcal{P}_{\text{M}\Gamma} + \Delta\mathcal{P}_{\text{M}'\text{K}} + \Delta\mathcal{P}_{\text{M}''\text{K}'}, \quad (4)$$

owing to the equality of the polarization at C_6 -related \mathbf{k}_{\perp} . The right-hand side of Eq. (4) is expressible as a certain Chern invariant. To see this, we define six loops $\{\gamma_{\mathbf{k}'_{\perp}}\}$ by varying k_z at fixed \mathbf{k}'_{\perp} , with orientations indicated by the green arrows in Fig. 1(a). The mutually-exclusive condition guarantees that the filled vector space associated to *any* point on $\{\gamma_{\mathbf{k}'_{\perp}}\}$ is identically equal to the zero-angular-momentum subspace, making the Chern number well defined over each of the three sheets illustrated in Fig. 1(a). For a sheet bounded by $\{\gamma_{\mathbf{k}'_{\perp}}, \gamma_{\mathbf{k}''_{\perp}}\}$, we define the associated Chern number as $\mathcal{C}_{\mathbf{k}'_{\perp}\mathbf{k}''_{\perp}}$; this quantity is identical [28] to the polarization difference $\Delta\mathcal{P}_{\mathbf{k}'_{\perp}\mathbf{k}''_{\perp}}$.

At the same time, viewing the Hamiltonian as a map from the BZ to the Bloch sphere of occupied, pseudospin-half wave functions, the six γ -loops are the preimage of the north pole of the Bloch sphere (corresponding to the $\ell=0$ state with $\langle\sigma_z\rangle=1$), and the three sheets are open Gaussian surfaces stretching over said preimage. This viewpoint allows us to apply Whitehead's formulation of the Hopf invariant [41], namely that χ equals the Chern number of the *oriented* surface stretched over the *oriented* preimage of *any* point of the Bloch sphere; note that the preimage generically forms one-dimensional loop(s) because \mathbf{k} -space is three-dimensional and the Bloch sphere two-dimensional [36]. The orientation of the preimage is defined to be anti-parallel to the tangential component of the Berry curvature ($\nabla \times \mathbf{A}$). We show in the Supplemental Material [34] that the sign of $(\nabla \times \mathbf{A})_z$ is determined by $\ell_c-\ell_v=1$ in our minimal model, which fixes the orientation (of the north-pole preimage) to coincide with the previously-specified orientation of the γ -loops [cf. Fig. 1(a)]. It follows that $\chi=\mathcal{C}_{\text{M}\Gamma}+\mathcal{C}_{\text{M}'\text{K}}+\mathcal{C}_{\text{M}''\text{K}'}$ by the Whitehead formula, and comparison with Eq. (4) gives the Hopf-RTP correspondence in Eq. (3) with \equiv_6 replaced by an exact equality. We have verified this equality for all $m\in\mathbb{R}$ in our minimal model by a direct calculation of χ via Eq. (2); the final result is presented in Fig. 1(b).

The \equiv_6 must be re-instated for the most general Pauli-matrix Hamiltonian that has trivial first Chern class and satisfies the mutually-exclusive condition (with $\ell_v=0, \ell_c=1$). The mod-six ambiguity arises from the possibility that the north-pole preimage not only comprises the six noncontractible γ -loops drawn in Fig. 1(a), but may also comprise contractible loops which must appear in multiples of six owing to six-fold symmetry; such contractible loops can be created by conduction-to-valence band touchings at generic \mathbf{k} .

The Chern numbers of the six contractible loops are identical ($=\mathcal{C}'$, say), in accordance with the pseudovector transformation of the Berry curvature. It follows from the Whitehead formula that $\chi = \mathcal{C}_{\text{M}\Gamma} + \mathcal{C}_{\text{M}'\text{K}} + \mathcal{C}_{\text{M}''\text{K}'} + 6\mathcal{C}'$, which differs from the RTP invariant $3\Delta\mathcal{P}_{\text{M}\Gamma} - 2\Delta\mathcal{P}_{\text{K}\Gamma}$ by an integer multiple of six. For completeness, other sources of the mod-six ambiguity are discussed in the Supplemental Material.

Bulk-boundary correspondence.— We have established the RTP and Hopf invariant as bulk delicate invariants leading to bulk multicellularity, but what does bulk multicellularity imply in the presence of a rotation-invariant surface termination? We answer with the following *obstruction principle*: there does not exist a symmetric, 2D tight-binding description (of a single surface facet) where all Wannier functions (in one unit cell) are centered on the same rotational axis as the bulk Wannier functions. Alternatively stated, on a half-infinite slab, the *entire* Hilbert space of states – filled and unfilled, bulk-extended and surface-localized – cannot be spanned by (uniaxially-symmetric, exponentially-localized) Wannier functions whose positional centers coincide with those Wannier functions obtained under periodic boundary conditions. We see that the nature of the Wannier obstruction is qualitatively dependent on the boundary condition.

A stronger form of this principle is realized by the half-infinite, Hopf-insulating slab (with or without rotational symmetry), namely that its Hilbert space does not even have an exponentially-localized Wannier representation; equivalently stated [3], the Hilbert space is characterized by a nonvanishing first Chern number – a stable, K -theoretic invariant [9]. This follows from the known bulk-boundary correspondence [33] of the Hopf insulator, which equates the bulk invariant χ with the *faceted Chern number* \mathcal{C}_f – defined as the net Chern number of all surface-localized bands, *independent* of filling. Figure 2(a) illustrates the topologically nontrivial surface-localized band with Chern number $\mathcal{C}_f = -1$ for our minimal model ($m=-6, \chi=-1$); note that surface-localized band(s) with the counter-balancing Chern number $\mathcal{C}'_f = +1$ do not exist in the entire Hilbert space (of filled and unfilled states) on a half-infinite geometry, and moreover the bulk bands have trivial first Chern class.

Next we demonstrate that the Hilbert space of a half-infinite RTP insulator either has no 2D tight-binding description (owing to stable or fragile topology), or has a 2D tight-binding description with displaced Wannier centers. To model an insulator that is not a Hopf insulator and yet has a nontrivial RTP, we enlarge the Hilbert space of our minimal model ($m=-6$) by adding a unicellular valence band whose representative Wannier function has angular momentum $\ell=2$. To simplify the discussion, we restrict ourselves to the $p3$ space group by including C_3 -symmetric (and C_2 -asymmetric) Hamiltonian matrix elements, while maintaining the bulk energy gap between conduction and valence bands. By construction, the mutually-exclusive condition is satisfied for representations of C_3 , thus the polarization difference $\Delta\mathcal{P}_{\text{K}\Gamma} = -1$ remains quantized, but quantization no longer holds for $\Delta\mathcal{P}_{\text{M}\Gamma}$.

For the bulk valence (VB) and conduction (CB) bands, the symmetry representations at C_3 -invariant wavevectors are presented in the first three rows of Fig. 2(c). For comparison, the

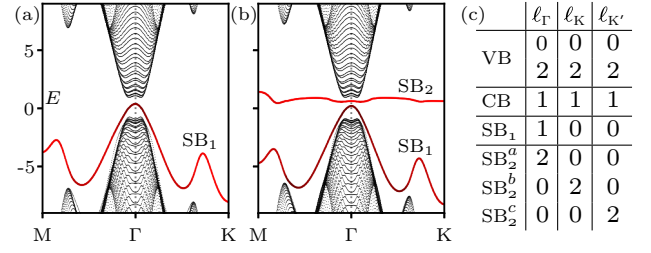


Figure 2. (a) Energy spectrum of a Hopf-insulating slab with bulk Hamiltonian given by Eq. (1); the surface Hamiltonian is modified so that the nontrivial surface band (red line) is detached from the bulk band [33]. (b) Spectrum of a slab of the RTP insulator [model (1) plus a unicellular valence band with $\ell=2$], with two detached surface bands. (c) For various bands discussed in the main text, ℓ_Γ , ℓ_K and $\ell_{K'}$ denote the mod-three angular momenta at C_3 -invariant wavevectors.

fourth row of Fig. 2(c) gives the symmetry representations of the nontrivial surface band SB₁ [cf. Fig. 2(b)], which is topologically equivalent to the nontrivial surface band of the minimal model in Fig. 2(a). Observe that the representations of SB₁ are identical to those of the bulk valence band *except* at Γ , where SB₁ has the same representation as the bulk conduction band. This is correlated [33] with the protrusion of the polarization $\mathcal{P}(\mathbf{k}_\perp)$ at Γ [cf. orange line in Fig. 1(c)].

We are ready to diagnose the advertised obstruction: being topologically nontrivial with Chern number $\mathcal{C}_f = -1$, SB₁ has no exponentially-localized Wannier representation. To attain such a representation, one must sum the surface band with another band (over the rBZ) having the opposite Chern number. Indeed, by modification of the surface Hamiltonian, one may always localize a second surface band SB₂ by detaching it (i.e., ‘peeling it off’) from either the bulk valence or bulk conduction band, as illustrated in Fig. 2(b). If detached from the conduction band, SB₂ combines bulk symmetry representations from the conduction subspace [third row in Fig. 2(c)], and such combination must respect all symmetry compatibility relations in \mathbf{k}_\perp -space [42]. Let us apply a rule for a C_3 -symmetric band with Chern number \mathcal{C} , namely that the product of C_3 eigenvalues at $\{\Gamma, K, K'\}$ gives $e^{-i2\pi\mathcal{C}/3}$ [43]. It follows that any detachment from the bulk conduction band necessarily has $\mathcal{C} \equiv_3 0$, and therefore cannot nullify the unit Chern number of SB₁. Instead, if we apply the same rule to detachments from the bulk *valence* band, there are only three possible symmetry representations for SB₂ compatible with $\mathcal{C}=+1$. The three possibilities, labelled SB₂^{a,b,c} in Fig. 2(c), are discussed in order.

Though a Wannier representation exists for the composite band SB₁⊕SB₂^a, these Wannier functions cannot individually be C_3 -symmetric on any of the C_3 -invariant Wyckoff positions: $\{1a, 1b, 1c\}$. Indeed, the symmetry representations of SB₁⊕SB₂^a are incompatible with a band representation of space group $P3$, which can be deduced by comparison with symmetry-representation tables in the Bilbao crystallographic server [44]. The obstruction to C_3 -symmetric Wannier functions is fragile, in the sense that a trivial band TB exists (though not necessarily in the present Hilbert space), such that SB₁⊕SB₂^a⊕TB is not obstructed.

In contrast, by comparing the symmetry representations of $SB_1 \oplus SB_2^b$ with the Bilbao tables, we deduce that $SB_1 \oplus SB_2^b$ does not have a fragile obstruction. Rather, it is a band representation with representative Wannier functions of angular momentum $\ell=1$ and $\ell=0$, centered on the $1c$ and $1a$ Wyckoff positions, respectively [34]; $SB_1 \oplus SB_2^c$ is likewise band-representable with $\ell=1$ and $\ell=0$, centered on $1b$ and $1a$, respectively. Indeed, no matter how many bands are detached from the bulk valence band and added to SB_1 , the resultant, composite band cannot have a tight-binding description with all Wannier centers on the $1a$ Wyckoff position of the bulk Wannier functions. Assuming the contrary, then the composite band satisfies a simple relation for its symmetry representations [7], namely that the set of C_3 eigenvalues are identical at Γ , K and K' . But this relation cannot be satisfied, because SB_1 contributes one C_3 eigenvalue ($=e^{i2\pi/3}$) at Γ which can never have an equal counterpart at K and K' .

Conclusion.— The multicellular landscape, as enriched by crystalline symmetries, promises to be fertile ground for topological insulators that would naively be missed and deemed trivial. We have introduced two (not necessarily disjoint) classes of multicellular, Wannierizable topological insulators: rotation-invariant insulators with a returning Thouless pump, and Hopf insulators. For these insulators, we have shown that bulk multicellularity (a) is a delicate topological invariant, and (b) implies that the Hilbert space (on a half-infinite slab) cannot be Wannierized with Wannier centers identical to those of the bulk Wannier functions (under periodic boundary con-

ditions). Whether (a–b) extend to *all* multicellular topological insulators is presently unanswered. Whether all delicate topological invariants (of the Berry-Zak phase, in quantum entanglement, of surface states, etc.) are accompanied by bulk multicellularity is also unknown.

The multicellular Hopf insulator is already known to manifest higher-order topology, quantized surface magnetism, and quantized magneto-electric polarizability [33]; it would be interesting to investigate if these properties extend to other multicellular/delicate topological insulators. Beyond band theory, we expect multicellularity to add a new chapter to the interplay between unlocalizable Wannier functions, generalized Hubbard models and exotic correlated phases; such interplay has previously only been explored for stable [45] and fragile [46, 47] topology.

Acknowledgments.— We thank A. Bouhon for alerting us to Whitehead’s formulation of the Hopf invariant. A. N. was supported by the Swiss National Science Foundation (SNSF) grant No. 176877, and by Forschungskredit of the University of Zurich, grant No. FK-20-098. T. N. acknowledges support from the European Research Council (ERC) under the European Unions Horizon 2020 research and innovation programme (ERC-StG-Neupert-757867-PARATOP) and from the NCCR MARVEL funded by the SNSF. T. B. was supported by the SNSF Ambizione grant No. 185806. A. A. was supported by the Gordon and Betty Moore Foundation EPiQS Initiative through Grant No. GBMF4305 at the University of Illinois.

-
- [1] D. J. Thouless, *J. Phys. Condens. Matter* **17**, L325 (1984).
 - [2] T. Thonhauser and D. Vanderbilt, *Phys. Rev. B* **74**, 235111 (2006).
 - [3] C. Brouder, G. Panati, M. Calandra, C. Mourougane, and N. Marzari, *Phys. Rev. Lett.* **98**, 046402 (2007).
 - [4] A. A. Soluyanov and D. Vanderbilt, *Phys. Rev. B* **83**, 035108 (2011).
 - [5] M. Taherinejad, K. F. Garrity, and D. Vanderbilt, *Phys. Rev. B* **89**, 115102 (2014).
 - [6] J. C. Budich, J. Eisert, E. J. Bergholtz, S. Diehl, and P. Zoller, *Phys. Rev. B* **90**, 115110 (2014).
 - [7] J. Höller and A. Alexandradinata, *Phys. Rev. B* **98**, 024310 (2018).
 - [8] N. Read, *Phys. Rev. B* **95**, 115309 (2017).
 - [9] A. Kitaev, *AIP Conf. Proc.* **1134**, 22 (2009).
 - [10] D. S. Freed and G. W. Moore, *Ann. Henri Poincaré* **14**, 1927 (2013).
 - [11] J. Kruthoff, J. de Boer, J. van Wezel, C. L. Kane, and R.-J. Slager, *Phys. Rev. X* **7**, 041069 (2017).
 - [12] K. Shiozaki, M. Sato, and K. Gomi, *Phys. Rev. B* **95**, 235425 (2017).
 - [13] H. C. Po, H. Watanabe, and A. Vishwanath, *Phys. Rev. Lett.* **121**, 126402 (2018).
 - [14] A. Bouhon, A. M. Black-Schaffer, and R.-J. Slager, *Phys. Rev. B* **100**, 195135 (2019).
 - [15] B. Bradlyn, Z. Wang, J. Cano, and B. A. Bernevig, *Phys. Rev. B* **99**, 045140 (2019).
 - [16] D. V. Else, H. C. Po, and H. Watanabe, *Phys. Rev. B* **99**, 125122 (2019).
 - [17] Z.-D. Song, L. Elcoro, Y.-F. Xu, N. Regnault, and B. A. Bernevig, *Phys. Rev. X* **10**, 031001 (2020).
 - [18] A. Alexandradinata, J. Höller, C. Wang, H. Cheng, and L. Lu, arXiv e-prints, arXiv:1908.08541 (2019), [arXiv:1908.08541](https://arxiv.org/abs/1908.08541) [cond-mat.str-el].
 - [19] B. Bradlyn, L. Elcoro, J. Cano, M. G. Vergniory, Z. Wang, C. Felser, M. I. Aroyo, and B. A. Bernevig, *Nature* **547**, 298 (2017), article.
 - [20] J. Cano, B. Bradlyn, Z. Wang, L. Elcoro, M. G. Vergniory, C. Felser, M. I. Aroyo, and B. A. Bernevig, *Phys. Rev. B* **97**, 035139 (2018).
 - [21] H. C. Po, A. Vishwanath, and H. Watanabe, *Nature Communications* **8**, 50 (2017).
 - [22] A. Alexandradinata and J. Höller, *Phys. Rev. B* **98**, 184305 (2018).
 - [23] J. Zak, *Phys. Rev. B* **23**, 2824 (1981).
 - [24] H. Bacry, *Commun. Math. Phys.* **153**, 359 (1993).
 - [25] A. P. Schnyder, S. Ryu, A. Furusaki, and A. W. W. Ludwig, *Phys. Rev. B* **78**, 195125 (2008).
 - [26] A. P. Schnyder, S. Ryu, A. Furusaki, and A. W. W. Ludwig, *AIP Conf. Proc.* **1134**, 10 (2009).
 - [27] N. Marzari and D. Vanderbilt, *Phys. Rev. B* **56**, 12847 (1997).
 - [28] A. Alexandradinata, X. Dai, and B. A. Bernevig, *Phys. Rev. B* **89**, 155114 (2014).
 - [29] G. H. Wannier, *Phys. Rev.* **117**, 432 (1960).
 - [30] J. Zak, *Phys. Rev. Lett.* **62**, 2747 (1989).
 - [31] R. D. King-Smith and D. Vanderbilt, *Phys. Rev. B* **47**, 1651 (1993).
 - [32] D. J. Thouless, *Phys. Rev. B* **27**, 6083 (1983).

- [33] A. Alexandradinata, A. Nelson, and A. A. Soluyanov, “Teleportation of Berry curvature on the surface of a Hopf insulator,” (2019), [arXiv:1910.10717 \[cond-mat.str-el\]](#).
- [34] The Supplemental Material, which includes Ref. [48], contains (i) information about the three-band and four-band models, (ii) proof of the RTP-Hopf relation, and (iii) a detailed analysis of the surface band representations and obstruction principle.
- [35] L. Pontrjagin, *Mat. Sb.* **9(51)**, 331 (1941).
- [36] R. Kennedy, *Phys. Rev. B* **94**, 035137 (2016).
- [37] J. E. Moore, Y. Ran, and X.-G. Wen, *Phys. Rev. Lett.* **101**, 186805 (2008).
- [38] H. Hopf, *Math. Ann.* **104**, 637 (1931).
- [39] F. Wilczek and A. Zee, *Phys. Rev. Lett.* **51**, 2250 (1983).
- [40] M. V. Berry, *Proc. R. Soc. Lond A* **392**, 45 (1984).
- [41] J. H. C. Whitehead, *Proc. Natl. Acad. Sci.* **33**, 117 (1947).
- [42] M. Tinkham, *Group Theory and Quantum Mechanics* (Dover, New York, 2003).
- [43] C. Fang, M. J. Gilbert, and B. A. Bernevig, *Phys. Rev. B* **86**, 115112 (2012).
- [44] L. Elcoro, B. Bradlyn, Z. Wang, M. G. Vergniory, J. Cano, C. Felser, B. A. Bernevig, D. Orobengoa, G. de la Flor, and M. I. Aroyo, *J. Appl. Crystallogr.* **50**, 1457 (2017).
- [45] J. S. Hofmann, E. Berg, and D. Chowdhury, “Superconductivity, pseudogap, and phase separation in topological flat bands: a quantum monte carlo study,” (2019), [arXiv:1912.08848 \[cond-mat.str-el\]](#).
- [46] J. Kang and O. Vafek, *Phys. Rev. Lett.* **122**, 246401 (2019).
- [47] V. Peri, Z. Song, B. A. Bernevig, and S. D. Huber, “Fragile topology and flat-band superconductivity in the strong-coupling regime,” (2020), [arXiv:2008.02288 \[cond-mat.supr-con\]](#).
- [48] X.L. Qi, Y.S. Wu, and S.C. Zhang, *Phys. Rev. B* **74**, 085308 (2006).

Supplemental Material to: Multicellularity of delicate topological insulators

Aleksandra Nelson,^{1,*} Titus Neupert,¹ Tomáš Bzdušek,^{2,1} and A. Alexandradinata³

¹*Department of Physics, University of Zurich, Winterthurerstrasse 190, 8057 Zurich, Switzerland*

²*Condensed Matter Theory Group, Paul Scherrer Institute, 5232 Villigen PSI, Switzerland*

³*Department of Physics, University of Illinois at Urbana-Champaign, Urbana, Illinois 61801-2918, USA*

CONTENTS

A. Stability of returning Thouless pump under addition of unicellular bands	1
B. RTP-Hopf mod-six correspondence	3
1. Review of Whitehead formulation of the Hopf invariant	3
2. Proof of the modulo-six RTP-Hopf correspondence	3
1. Assigning orientations to preimage loops	4
2. Assuming the north-pole preimage comprises only rotation-invariant lines	5
3. Assuming the north-pole preimage comprises more than the rotation-invariant lines	5
C. Strong obstruction principle for the Hopf insulator	7
1. Proof of obstruction principle	7
2. Delicacy of obstruction principle	7
D. Decomposition of surface bands of the $P3$ -symmetric model into band representations	8
E. Finite slab models	8
1. Hamiltonian for a slab geometry	8
2. Algorithm to detach a surface state	9

A. STABILITY OF RETURNING THOULESS PUMP UNDER ADDITION OF UNICELLULAR BANDS

We numerically analyze the stability of RTP under addition of a unicellular conduction band whose Wannier representatives transform in one-dimensional representations of rotation. As a starting model that possesses an RTP we use the minimal model (1) of the main text with a parameter value $m = -6$, which corresponds to $\Delta \mathcal{P}_{M\Gamma} = -1$ and $\Delta \mathcal{P}_{K\Gamma} = -1$. Its returning Thouless pump (RTP) is shown in Fig. S1(a) by solid orange line. To better track the changes in polarization, we focus in Fig. S1(b-d) on the small neighborhoods of the rotation-invariant points M, Γ and K, respectively, which correspond to dashed rectangles in Fig. S1(a). The non-minimal models with additional band are described with the following tight-binding Hamiltonian:

$$H_3 = \left(\begin{array}{c|c} H(\mathbf{k}) & \begin{matrix} h_{vc'}(\mathbf{k}) \\ h_{cc'}(\mathbf{k}) \end{matrix} \\ \hline \begin{matrix} h_{vc'}(\mathbf{k})^* & h_{cc'}^*(\mathbf{k}) \end{matrix} & E(\mathbf{k}) \end{array} \right), \quad (\text{S1})$$

where $H(\mathbf{k})$ the minimal model in Eq. (1), $E(\mathbf{k})$ is the energy dispersion of the added band (absent inter-band hybridization), and $h_{vc'}(\mathbf{k})$ [resp. $h_{cc'}(\mathbf{k})$] describes the coupling between the added band and the valence s -type (resp. conduction p_+ -type) band of the original model. In all tests, an on-site potential is chosen for the added orbital such that $E(\mathbf{k}) = 50$, which is smaller than the bandwidth Δ of the minimal model ($\Delta = 338$, defined as the difference between the maximum energy of the conduction band and the minimum energy of the valence band). By fixing the angular momentum ℓ'_c of the added band we impose the following constraint on the Hamiltonian

$$R_{C_6} H_3(\mathbf{k}) R_{C_6}^{-1} = H_3(C_6 \mathbf{k}), \quad R_{C_6} = \begin{pmatrix} 1 & 0 & 0 \\ 0 & e^{i2\pi/6} & 0 \\ 0 & 0 & e^{i2\pi\ell'_c/6} \end{pmatrix}. \quad (\text{S2})$$

* anelson@physik.uzh.ch

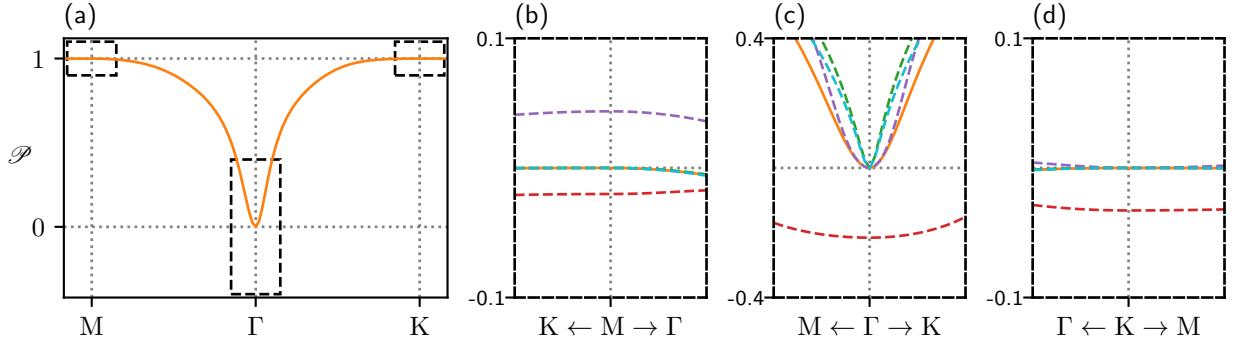


Figure S1. (a) RTP for the two-band model of Eq. (1) of the main text at $m = -6$. Three zoom-in rectangles are shown, which correspond to panels (b–d), where RTP of the two-band model is compared against RTP of multi-band models described in Sec. A. Solid orange line indicates the original two-band model (1) with angular momenta $\ell_v = 0$ and $\ell_c = 1$. Three-band models with additional conduction band with angular momenta $\ell'_c = 1$, $\ell'_c = 0$, and $\ell'_c = 2$ [captured by Eqs. (S1–S5)] are plotted, respectively, by dashed green/red/purple lines. The RTP of a four-band model [Eqs. (S6–S7)] with additional valence band with angular momentum $\ell'_v = 0$ and additional conduction band with $\ell'_c = 1$ is displayed with by dashed blue line.

First, we add a conduction band which transforms in the same representation as the original conduction band $\ell'_c = 1$. The symmetry constraint (S2) is fulfilled by setting

$$h_{vc'}(\mathbf{k}) = 1.5(\cos k_z + 2i \sin k_z) \cdot f_{-1}(k_x, k_y), \quad (\text{S3a})$$

$$h_{cc'}(\mathbf{k}) = 1.5i \cdot f_0(k_x, k_y), \quad (\text{S3b})$$

$$f_t(k_x, k_y) = \sum_{a=1}^6 \exp(i\pi t a/3) \cdot \exp\{i[\cos(\pi a/3)k_x + \sin(\pi a/3)k_y]\}. \quad (\text{S3c})$$

Such a band does not mix with the valence subspace and preserves the quantization of RTP [green dashed line in Fig. S1(b-d)]. In contrast, when the additional conduction band has $\ell'_c = 0$, matching the eigenvalue of the valence band, the quantization of RTP is lost at all high-symmetry points [red dashed line in Fig. S1(b-d)]. This is achieved by

$$h_{vc'}(\mathbf{k}) = 3(2 \cos k_z - 3i \sin k_z) \cdot f_0(k_x, k_y), \quad (\text{S4a})$$

$$h_{cc'}(\mathbf{k}) = 0 \quad (\text{S4b})$$

with $f_0(k_x, k_y)$ defined by Eq. (S3c) above.

When the representation of the additional conduction band is set to $\ell'_c = 2$ by choosing

$$h_{vc'}(\mathbf{k}) = 3(\cos k_z + 4i \sin k_z) \cdot f_{-2}(k_x, k_y), \quad (\text{S5a})$$

$$h_{cc'}(\mathbf{k}) = 3(\cos k_z + 3i \sin k_z) \cdot f_{-1}(k_x, k_y), \quad (\text{S5b})$$

its angular momentum coincides with that of the valence subspace at C_2 -invariant points. This reflects the fact that if we view the model as C_2 -symmetric (forgetting its C_6 symmetry), the mutually-exclusive condition is not satisfied, hence the polarization difference along ΓM is no longer integer-quantized. On the other hand, if the model is viewed as C_3 -symmetric, the mutually-exclusive condition is satisfied, hence the RTP along ΓK remains quantized [purple dashed line in Fig. S1(b-d)].

Additionally, we consider a four-band model where bands added to both valence and conduction subspaces keep the mutually-exclusive condition, having $\ell'_v = 0$ and $\ell'_c = 1$. It is given by a tight-binding Hamiltonian

$$H_4(\mathbf{k}) = \begin{pmatrix} -E(\mathbf{k}) & h_{v'v}(\mathbf{k}) & h_{v'c}(\mathbf{k}) & 0 \\ h_{v'v}^*(\mathbf{k}) & & & \\ h_{v'c}^*(\mathbf{k}) & H(\mathbf{k}) & & h_{v'c'}(\mathbf{k}) \\ 0 & h_{v'c'}^*(\mathbf{k}) & h_{cc'}^*(\mathbf{k}) & E(\mathbf{k}) \end{pmatrix}, \quad (\text{S6})$$

with the same choice of $E(\mathbf{k}) = 50$, and with further matrix elements

$$h_{v'v}(\mathbf{k}) = \exp(ik_z) f_0(k_x, k_y), \quad (\text{S7a})$$

$$h_{v'c}(\mathbf{k}) = -2(\cos k_z - i \sin k_z) \cdot f_{-1}(k_x, k_y), \quad (\text{S7b})$$

$$h_{vc'}(\mathbf{k}) = (\cos k_z + 2i \sin k_z) \cdot f_{-1}(k_x, k_y), \quad (\text{S7c})$$

$$h_{cc'}(\mathbf{k}) = \exp(ik_z) \cdot f_0(k_x, k_y), \quad (\text{S7d})$$

that satisfy the symmetry constraint

$$R_{C_6} H_4(\mathbf{k}) R_{C_6}^{-1} = H_4(C_6 \mathbf{k}), \quad R_{C_6} = \begin{pmatrix} 1 & 0 & 0 & 0 \\ 0 & 1 & 0 & 0 \\ 0 & 0 & e^{i2\pi/6} & 0 \\ 0 & 0 & 0 & e^{i2\pi/6} \end{pmatrix}. \quad (\text{S8})$$

We observe that the RTP remains quantized [blue dashed line in Fig. S1(b-d)] under the addition of uniaxial valence and conduction bands that respect the mutually-exclusive condition. The presented study of RTP stability illustrates the notion of symmetry-protected delicate topology.

B. RTP-HOPF MOD-SIX CORRESPONDENCE

We elaborate on a proof of the RTP-Hopf mod-six correspondence [Eq. (3) of the main text], which has only been sketched in the main text. We remind the reader that the correspondence holds for any C_6 -symmetric, Pauli-matrix Hamiltonian with trivial first Chern class and with the property that representative Wannier functions of the valence and conduction bands are centered on the C_6 -symmetric Wyckoff position, and transform (under C_6) with angular momenta $\ell_v = 0$ and $\ell_c = 1$, respectively. Our proof utilizes an equivalent formula for the Hopf invariant derived by Whitehead [41], which we briefly review.

1. Review of Whitehead formulation of the Hopf invariant

We view the Hopf-insulating Hamiltonian $H(\mathbf{k})$ as a map from a Brillouin zone (BZ) three-torus to a Bloch sphere of occupied pseudospin-half vectors (or, equivalently, into the classifying space of 2-band Hamiltonians, $U(2)/U(1) \times U(1) \cong S^2$):

$$H : \mathbf{k} \mapsto -z^\dagger(\mathbf{k}) \boldsymbol{\sigma} z(\mathbf{k}) \quad (\text{S9})$$

We assume the map has trivial first Chern class, thus excluding the Hopf-Chern insulators introduced in Ref. 36. In this case, the preimage of any point x_0 on a Bloch sphere is an orientable (but not necessarily path-connected) path in BZ:

$$H^{-1}(x_0 \in S^2) = \bigcup_i \gamma_i, \quad (\text{S10})$$

with orientation defined to be anti-parallel to the tangential component of the Berry curvature; being anti-parallel rather than parallel is a matter of convention. Possible preimage paths γ_i are illustrated in Fig. S2(a) by green lines: γ_1 is a closed loop while γ_2 consists of two non-contractible loops winding around the BZ torus. That the two non-contractible loops have opposite orientation is not an accident, and is a result of pairing rule derived in Sec. B 2 1.

Whitehead showed that the Hopf invariant coincides with the Chern number \mathcal{C} on the oriented open Gaussian surface Σ (so-called *Seifert surface*) whose boundary is the preimage path, $\partial \Sigma = \bigcup_i \gamma_i$, i.e.

$$\chi = \mathcal{C}_\Sigma := \frac{1}{2\pi} \int_\Sigma \mathcal{F} \cdot d\Sigma, \quad (\text{S11})$$

with \mathcal{F} the Berry curvature of the filled band. Note that the Chern number is well-defined *and quantized*, because the wave function (of the filled band) is constant on the preimage $\bigcup_i \gamma_i$, hence the surface Σ can be treated as closed.

2. Proof of the modulo-six RTP-Hopf correspondence

For the class of C_6 -invariant Hamiltonians considered in the main text, we choose, without loss of generality, a basis such that the $\ell = 0$ (resp. $\ell = 1$) state corresponds to the expectation value $\langle \sigma_z \rangle = 1$ ($\langle \sigma_z \rangle = -1$). The symmetry constraint on the Hamiltonian is then

$$R_{C_6} H(\mathbf{k}) R_{C_6}^{-1} = H(C_6 \mathbf{k}), \quad R_{C_6} = \begin{pmatrix} 1 & 0 \\ 0 & \exp(i2\pi/6) \end{pmatrix} \quad (\text{S12})$$

By assumption, the valence-band energy eigenvector at all rotation-invariant lines of the BZ belongs to the one-dimensional $\ell = 0$ subspace, hence all these lines belong to the preimage of the north pole on the Bloch sphere. We denote the C_6, C_3, C_2 -invariant lines by $\gamma_\Gamma, \{\gamma_K, \gamma_{K'}\}$ and $\{\gamma_M, \gamma_{M'}, \gamma_{M''}\}$, respectively, as illustrated by green lines in Fig. S2(b). Note that lines $\gamma_{K,K'}$ and $\gamma_{M,M',M''}$ are mutually related by C_6 rotation.

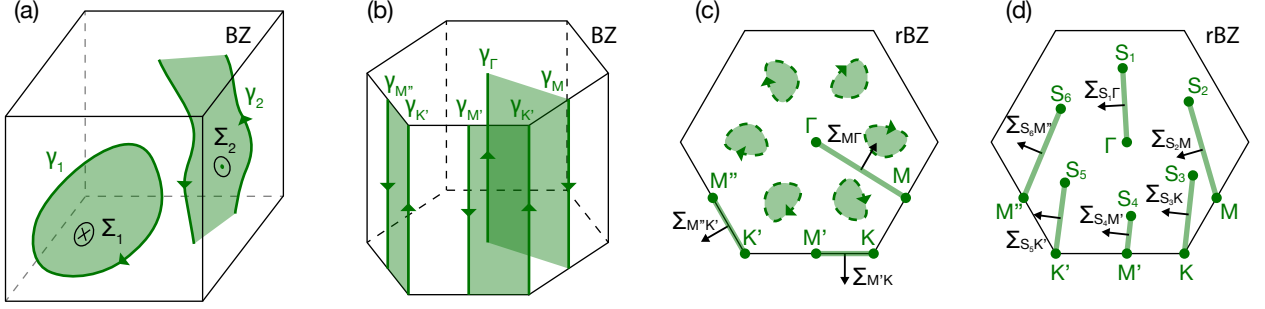


Figure S2. (a) Oriented preimage $H^{-1}(x_0) = \gamma_1 \cup \gamma_2$ inside the Brillouin zone (BZ) of a point x_0 on a Bloch sphere, assuming a generic two-band (Pauli-matrix) Hamiltonian. The sheet $\Sigma_1 \cup \Sigma_2$ is an oriented surface stretched over the preimage, with orientation defined using the right-hand rule. (b) In a C_6 -invariant model with $\ell_c = 1$ and $\ell_v = 0$, the rotation-invariant lines $\gamma_\Gamma, \gamma_K, \gamma_{K'}, \gamma_M, \gamma_{M'}$ and $\gamma_{M''}$ are preimages of the north pole on the Bloch sphere. Their orientation is defined anti-parallel to the tangent component of Berry curvature. (c) Projection into the reduced Brillouin zone (rBZ); this includes the projection of surfaces $\Sigma_{M\Gamma}, \Sigma_{M'K}$ and $\Sigma_{M''K'}$ stretched over the six rotation invariant lines, with orientations indicated by the black arrows. Additional possible preimages that appear in six copies related by C_6 are illustrated. (d) Additional preimages in the form of six non-contractible lines are denoted by S_i in the projection to rBZ. Surfaces that are stretched over the full preimage are denoted as $\Sigma_{S_1\Gamma}, \Sigma_{S_3K}, \Sigma_{S_5K'}, \Sigma_{S_2M}, \Sigma_{S_4M'}$ and $\Sigma_{S_6M''}$.

1. Assigning orientations to preimage loops

We assign orientation to all $\{\gamma_{k_\perp}\}$ in accordance with the following rules:

- (i) *Pairing rule*: any intersection of a 2D BZ subtorus with the preimage (of any single point on the Bloch sphere) must come in pairs with opposite orientation.
- (ii) If γ_{k_\perp} and $\gamma_{k'_\perp}$ are related by rotation, they must have the same orientation (owing to the Berry curvature transforming under spatial transformations as a pseudovector).
- (iii) The orientations of $\gamma_{\Gamma,K,K'}$ point upwards (as derived from the difference between conduction and valence angular momenta, $\ell_c - \ell_v = 1$, in a paragraph below).

Derivation of pairing rule.— Our assumption of a trivial first Chern class means that the first Chern number vanishes on any 2D cut of the BZ, and in particular it vanishes for all 2D subtori T^2 of the BZ. Parametrizing T^2 by (k_x, k_y) and defining k_z by the right-hand rule, the Chern number is given by the following integral of the Berry curvature: $\mathcal{C} = (2\pi)^{-1} \int_{T^2} \mathcal{F}_z dk_x dk_y$. Recall that the first Chern number \mathcal{C} of a pseudospinor Hamiltonian defined on T^2 tells how many times this manifold wraps around the Bloch sphere under the Hamiltonian map $H : T^2 \rightarrow S^2$. If $\mathcal{C} = 0$, then any point x_0 on the Bloch sphere must be visited an even number of times as one sweeps through T^2 , i.e., the preimage of x_0 consists of an even number of points $\{k_1, \dots, k_{2N}\}$ in T^2 . Let us define $d_{x_0} \in S^2$ as an infinitesimal outward (i.e., positively) oriented disk centered at x_0 , and $\delta\Omega_{x_0} > 0$ as the solid angle subtended by d_{x_0} . The preimage of d_{x_0} comprises $2N$ disks $\{D_1, \dots, D_{2N}\}$ encircling $\{k_1, \dots, k_{2N}\}$, respectively, with orientations inherited from T^2 . We now assign each D_j an index, $\text{ind}[D_j] = \pm 1$, by checking whether $H(\partial D_j)$ (with the orientation of the boundary determined by right-hand rule) is parallel or antiparallel to the oriented boundary $(\partial d_{x_0}) \subset S^2$ [i.e., whether it winds (counter-)clockwise around the north pole]. Applying the solid-angle interpretation of the Berry phase for pseudospinor Hamiltonians [40], the Berry curvature integrated over the oriented disk D_j equals $\text{ind}[D_j] \delta\Omega_{x_0}/2$. (This equality also manifests that $-\text{ind}[D_j] = -\text{sgn}[F_z(k_j)]$, which is the definition of the preimage orientation adopted in the main text.) Because d_{x_0} is covered by the map $(H : T^2 \rightarrow S^2)$ a number of times equal to the Chern number (assumed zero), the net Berry curvature integrated over $\{D_1, \dots, D_{2N}\}$ must vanish, implying that N of $\{D_1, \dots, D_{2N}\}$ have index opposite to the remaining N disks. This completes the proof.

The remainder of this subsection is used to derive rule (iii), which follows from the assumed angular momenta ($\ell_v = 0$ and $\ell_c = 1$) and from a $\mathbf{k} \cdot \mathbf{p}$ analysis at the C_3 -invariant wavevectors. (Note, however, that the little groups of $\{M, M', M''\}$ are not sufficiently constraining to determine the orientations of $\gamma_{M,M',M''}$.) Since the preimage orientation depends only on the Berry curvature (a property of the wave function), it may as well be determined by the spectrally-flattened Hamiltonian. By assumption, such a ‘flat-band’ Hamiltonian at rotation-invariant lines is $H = \mathbf{1} - 2(1, 0)^T(1, 0) = -\sigma_z$, with $\mathbf{1}$ the identity matrix.

Moving slightly away from γ_Γ (or $\gamma_{K,K'}$), the leading-order correction to this Hamiltonian is determined from Eq. (S12) to be

$$H(\mathbf{k}) = h_+ \sigma_+ + h_- \sigma_- + h_z \sigma_z, \quad (h_+, h_-, h_z) = (ak_-, a^* k_+, -1), \quad k_\pm = k_x \pm ik_y, \quad \sigma_\pm = \sigma_x \pm i\sigma_y, \quad a \in \mathbb{C}. \quad (\text{S13})$$

In general, the filled-band Berry curvature of a two-by-two, flat-band Hamiltonian, $H(\mathbf{k}) = \sum_{i=1}^3 q_i(\mathbf{k}) \sigma_i$ with $\|\mathbf{q}\| = 1$, is expressible as a skyrmion density [48]:

$$\mathcal{F}_z = \frac{1}{2} \epsilon_{ijk} q_i \partial_x q_j \partial_y q_k \quad (\text{S14})$$

In the particular case that q_3 is independent of k_x and k_y , the general expression reduces to

$$\mathcal{F}_z = \frac{1}{2} q_3 (\partial_x q_1 \partial_y q_2 - \partial_x q_2 \partial_y q_1) = -2h_z (\partial_+ h_+ \partial_- h_- - \partial_+ h_- \partial_- h_+) + O(k_\perp^2), \quad \partial_\pm = \frac{1}{2} (\partial_{k_x} \mp i\partial_{k_y}). \quad (\text{S15})$$

In the last step, we substituted $h_z = q_3 + O(k_\perp^2)$ and $2h_\pm = q_1 \mp iq_2 + O(k_\perp^2)$, with $O(k_\perp^2)$ terms resulting from having to normalize $\|\mathbf{q}\| = 1$. Substituting the expressions for $\{h_j\}_{j \in \{+, -, z\}}$ from Eq. (S13) into Eq. (S15), we obtain $\mathcal{F}_z = -2|a|^2 + O(k_\perp^2)$. The orientation of the preimage (at C_3 -invariant \mathbf{k}) is defined to be anti-parallel to $(0, 0, \mathcal{F}_z)$, hence the three upward-facing arrows at $\gamma_\Gamma, \gamma_K, \gamma_{K'}$ displayed in Fig. S2(b).

If we had chosen a different basis where $\ell = 0$ (resp. $\ell = 1$) state has expectation $\langle \sigma_z \rangle = -1$ ($\langle \sigma_z \rangle = 1$), while fixing the valence subspace to have zero angular momentum, then an analogous symmetry analysis gives $(h_+, h_-, h_z) = (a^* k_+, ak_-, 1)$, which gives the same value for \mathcal{F}_z , and hence also the same orientation for the preimage at C_3 -invariant \mathbf{k} .

2. Assuming the north-pole preimage comprises only rotation-invariant lines

Postponing the more general situation to a subsequent subsection, let us first assume that the north-pole preimage comprises only the rotation-invariant lines, as is indeed true for the minimal model in the main text. These lines intersect the $k_z = 0$ subtorus at six points, allowing us to apply rule (i) from Sec. B 2.1. Combining with rule (iii), we deduce that the three γ_M lines are *downward* oriented [cf. Fig. S2(b)], as is consistent with rule (ii). A possible choice for oriented surfaces bounded by the six γ lines are the three light-green sheets in Fig. S2(b), which we denote by $\Sigma_{M\Gamma}$, $\Sigma_{M'K}$ and $\Sigma_{M''K'}$; the orientation of these surfaces are determined by the right-hand rule, as shown by black arrows in Fig. S2(c). The Chern number contributed by the oriented surface $\Sigma_{K'_\perp K''_\perp}$ is the difference in polarization between upward- and downward-oriented edges, $\mathcal{C}_{K'_\perp K''_\perp} = \mathcal{P}_{K''_\perp} - \mathcal{P}_{K'_\perp}$, assuming that the polarization is continuously defined over the reduced Brillouin zone (rBZ). Finally, applying the Whitehead formula in Eq. (S11), and the equality of \mathcal{P} at symmetry-related \mathbf{k}'_\perp , we derive the exact equality: $\chi = 2\Delta\mathcal{P}_{MK} + \Delta\mathcal{P}_{M\Gamma} = 3\Delta\mathcal{P}_{M\Gamma} - 2\Delta\mathcal{P}_{K\Gamma}$, in accordance with Eq. (3) of the main text.

3. Assuming the north-pole preimage comprises more than the rotation-invariant lines

If the north-pole preimage comprises more than the rotation-invariant lines, then the RTP-Hopf relation is generalized to

$$\chi \equiv_6 2\Delta\mathcal{P}_{MK} + \Delta\mathcal{P}_{M\Gamma}. \quad (\text{S16})$$

There are five classes of possibilities for additional preimages, with the last three involving a nontrivial linking of the preimage loops:

- (i) They can form contractible loops as in Fig. S2(c) which always appear in six copies related by C_6 symmetry, thus possibly changing the RTP-Hopf relation by an integer multiple of six (this is discussed in the main text).
- (ii) Additional preimages can extend across the BZ in the form of six rotation-related lines γ_{S_i} as illustrated in Fig. S2(d). To satisfy the pairing rule, the orientations of C_2 -invariant lines γ_M must be upward-oriented, while all γ_S lines are downward-oriented. The oriented surfaces which contribute to Hopf invariant are $\Sigma_{S_1\Gamma}$, Σ_{S_3K} , $\Sigma_{S_5K'}$, Σ_{S_2M} , $\Sigma_{S_4M'}$ and $\Sigma_{S_6M''}$, as illustrated in Fig. S2(d).
- (iii) A preimage loop may link with (i.e., encircle) the non-contractible γ_Γ -loop.

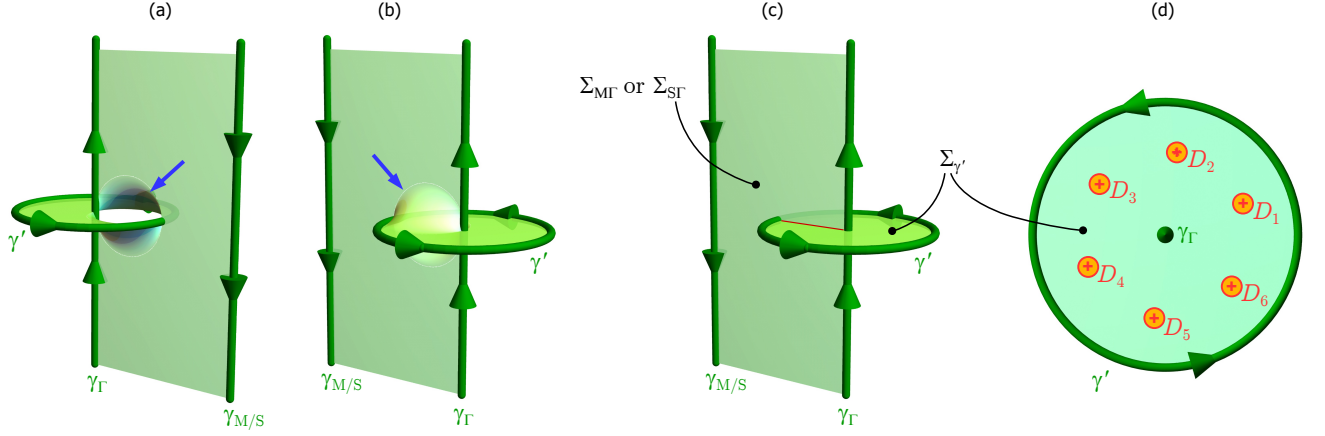


Figure S3. Illustrations for case (iii) of additional preimages, as listed in Sec. B 2.3. All oriented lines are components of $\bigcup_i \gamma_i = H^{-1}(\sigma_z)$. (a,b) Two views (back vs. front) of a smooth open Gaussian surface (pale green) bounded by non-contractible paths γ_Γ and $\gamma_{M/S}$, and by a contractible path γ' that is linked with γ_Γ (oriented green lines). The inscribed sheet is flat everywhere, except for a small inflection region indicated by blue arrow. (c) By continuously shrinking the inflection region, one can effectively deform the inscribed surface into a pair of flat sheets (labelled $\Sigma_{M\Gamma}/\Sigma_{S\Gamma}$ and $\Sigma_{\gamma'}$) that cross along the red line. (d) The Chern number on $\Sigma_{\gamma'}$ is determined by counting the indices $\text{ind}[D_j]$ (set to “+” in the figure) of preimages of a small neighborhood of the *south* pole $-\sigma_z \in S^2$. Due to C_6 -symmetry, these appear in multiples of six, $\{D_j\}_{j=1}^6$ (orange disks), with the same index. It follows that the Chern number $\mathcal{C}_{\gamma'}$ is an integer multiple of six.

(iv) A preimage loop may link with the γ_K -loop, alongside a C_2 -related loop that links with the $\gamma_{K'}$ -loop.

(v) A preimage loop may link with the γ_M -loop, with a C_3 -related (resp. C_3^{-1} -related) loop linking with the $\gamma_{M'}$ -loop (resp. $\gamma_{M''}$ -loop).

Let us prove Eq. (S16) for cases (ii-v) in turn.

For case (ii), the six non-contractible loops at generic wavevectors are generally curvilinear. The parallel transport of Bloch wave functions along each non-contractible loop defines a Zak phase $\phi_Z(S_j)$ (as the line integral of the Berry-Zak connection); the geometric theory of polarization gives $\phi_Z(S_j)/2\pi \equiv \mathcal{P}(S_j)$ *only for straight* non-contractible loops. However, observe that the eigenvector of $H(\mathbf{k})$ is constant along γ_{S_j} , with said constant vector being the zero-angular-momentum state. It thus follows that the Zak phase reduces [7] to $\phi_Z/2\pi \equiv \mathbf{G} \cdot \mathbf{w}$, with \mathbf{G} the reciprocal vector connecting the intersection of γ_{S_j} with the BZ boundary, and \mathbf{w} the central position of a representative, zero-angular-momentum Wannier function. We have already established in the main text that $\mathcal{P}(\mathbf{k}'_\perp) \equiv \mathbf{G} \cdot \mathbf{w}$, thus $\mathcal{P}(\mathbf{k}'_\perp) - \phi_Z(S_j)/2\pi \in \mathbb{Z}$. The six-fold symmetry guarantees that $\phi_Z(S_j)$ is independent of j , assuming the Bloch wave function is analytic and periodic over the Brillouin zone – a condition readily satisfied because of the triviality of the first Chern class.

Applying the Whitehead formula, as well as the equality of polarization (or the Zak phase) for C_6 -related loops, we obtain

$$\chi = \mathcal{P}(\Gamma) + 2\mathcal{P}(\mathbf{K}) + 3\mathcal{P}(\mathbf{M}) - 6\phi_Z(\mathbf{S})/2\pi. \quad (\text{S17})$$

The integer quantization of $\mathcal{P}(\mathbf{M}) - \phi_Z(\mathbf{S})/2\pi$ allows to substitute $[3\mathcal{P}(\mathbf{M}) - 6\phi_Z(\mathbf{S})/2\pi \equiv_6 -3\mathcal{P}(\mathbf{M})]$ in Eq. (S17), leading to the desired relation in Eq. (S16).

For case (iii) with a preimage loop γ' encircling γ_Γ , a smooth open Gaussian surface bounded by γ' and γ_Γ [Fig. S3(a,b)] may be continuously deformed, and then split into two intersecting surfaces [Fig. S3(c)]: one, denoted $\Sigma_{\gamma'}$, being C_6 -symmetric and bounded by γ' *alone*, and the other surface being C_6 -asymmetric and bounded on one side by γ_Γ [more precisely, it is either $\Sigma_{S,\Gamma}$ in Fig. S2(c) or $\Sigma_{M\Gamma}$ in Fig. S2(d)]. The contribution to χ by the second surface has already been analyzed in cases (i) and (ii) above, resp. in Sec. B 2.2. It thus remains to prove that $\Sigma_{\gamma'}$ can only contribute an integer multiple of six to χ .

To prove that Chern number $\mathcal{C}_{\gamma'}$ on the C_6 -symmetric surface $\Sigma_{\gamma'}$ is quantized to integer multiples of six, we utilize the concepts developed while deriving the pairing rule in Sec. B 2.1. We remind the reader that γ' belongs to the preimage of the north pole $(+\sigma_z)$ on the Bloch sphere; it is convenient to also consider the preimage of the *south* pole, $H^{-1}(-\sigma_z)$. Owing to the matrix representation of C_6 being simultaneously diagonal with σ_z , it follows that both $H^{-1}(\sigma_z)$ and $H^{-1}(-\sigma_z)$ are C_6 -symmetric; note this symmetry also extends to the orientations of said preimage, because of the pseudovector transformation of the Berry

curvature. (We remark that C_6 symmetry is generically not a property of the preimages of other points $x_0 \in S^2$.) It follows from the discussion in Sec. B 2.1 that $\mathcal{C}_{\gamma'} = \sum_j \text{ind}[D_j]$, where $D_j \subset \Sigma_{\gamma'}$ are preimages of a small neighborhood $d_{-\sigma_z} \subset S^2$ of the south pole. As both $\Sigma_{\gamma'}$ and $H^{-1}(-\sigma_z)$ are C_6 -symmetric, it follows that the preimages D_j (which cannot lie at γ_{Γ} because $H(\gamma_{\Gamma}) = +\sigma_z$) come in multiples of six, with all members of the sextuplet having the same index [Fig. S3(d)]. As a consequence, the contribution of the preimage γ' to χ is $\mathcal{C}_{\gamma'} \equiv_6 0$, thus preserving the validity of Eq. (S16).

The cases (iv) and (v) are analyzed with analogous arguments as those presented above for (iii). In the case (iv) of a pair of loops $\gamma'_{1,2}$ encircling K resp. K', one ends up considering a pair of surfaces $\Sigma_{\gamma'_{1,2}}$, each stretched along one of the two loops. It follows from the symmetry that the Chern numbers on the two surfaces are $\mathcal{C}_{\gamma'_1} = \mathcal{C}_{\gamma'_2} \equiv_3 0$. Therefore, their net contribution to χ is a multiple of six, thus preserving the validity of Eq. (S16). Similarly, the three symmetry-related loops $\gamma'_{1,2,3}$ that arise in case (v) lead us to consider three symmetry-related open Gaussian surfaces $\Sigma_{\gamma'_{1,2,3}}$, each carrying $\mathcal{C}_{\gamma'_i} \equiv_2 0$. It again follows that the net contribution of the additional preimages to χ is a multiple of six.

C. STRONG OBSTRUCTION PRINCIPLE FOR THE HOPF INSULATOR

The strong obstruction principle for the Hopf insulator states that there is no exponentially-localized Wannier representation for the Hilbert space of states defined on a half-infinite slab. We have claimed that this Hilbert space includes all states, independent of their filling and spatial extension. The meaning of this Hilbert space will be precisely established here, to complement the heuristic description given in the main text. Once the meaning is established, we will be able to prove the strong obstruction principle with greater rigor.

1. Proof of obstruction principle

By assumption of the triviality of the first Chern class, any surface-localized band (if it exists) can always be removed from the Fermi level by a deformation of the surface Hamiltonian. This implies the existence of an energy gap separating a filled subspace (defining the projector P) and unfilled subspace (with orthogonal projector Q). We then consider Bloch-Wannier eigenstates of $P\hat{z}P$ and $Q\hat{z}Q$, with eigenvalues of \hat{z} taking only positive values. We will see that adopting the Bloch-Wannier representation is not just a convenient choice of basis, it also allows to define the Hilbert space on a semi-infinite geometry.

We label the “filled” Bloch-Wannier eigenbands of $P\hat{z}P$ by an index $b=1, 2, \dots, b_{\max}-1, b_{\max}, b_{\max}+1, \dots$, such that band b lies closer (to the surface termination) than band b' , if $b < b'$. We impose that b_{\max} is sufficiently large, such that the Bloch-Wannier band with the same index is bulk-like, i.e., it is indistinguishable (up to exponentially small corrections) from a bulk Bloch-Wannier band defined with periodic boundary conditions. In particular, this means that band b_{\max} is related to $b_{\max} \pm 1$ by a discrete translation mapping $z \rightarrow z \pm 1$. We define the filled Hilbert space $\mathcal{H}_P[b_{\max}]$ as the set of Bloch-Wannier bands labelled by $b=1, 2, \dots, b_{\max}$. By similar consideration of the “unfilled” eigenbands of $Q\hat{z}Q$, we define the unfilled Hilbert space $\mathcal{H}_Q[b_{\max}]$ with the same truncation b_{\max} . The full Hilbert space of states on a half-infinite geometry is given by $\mathcal{H}_{1/2} = \mathcal{H}_P \oplus \mathcal{H}_Q$, with b_{\max} taken sequentially to infinity. This procedure of defining an infinite-dimensional Hilbert space by sequential embeddings in increasingly larger Hilbert spaces is not unlike the direct-limit procedure employed in K -theory [9].

We then compute the Chern number $\mathcal{C}_P(b)$ of each band as an integral of the Berry curvature over the rBZ, and define the sum $\mathcal{C}_P[B] = \sum_{b=1}^B \mathcal{C}_P(b)$. Viewed as a sequence in B , $\mathcal{C}_P[B]$ has a unique accumulation point (defined as \mathcal{C}_P) for large enough B (satisfying $B < b_{\max}$), because all bulk Bloch-Wannier bands have trivial Chern number owing to the bulk translational symmetry; \mathcal{C}_P has the physical meaning of the Chern number of filled Bloch-Wannier bands localized to a finite vicinity of the surface. We analogously define \mathcal{C}_Q as the Chern number of unfilled, surface-localized Bloch-Wannier bands. The net Chern number of all surface-localized bands, independent of filling, is then $\mathcal{C}_f = \mathcal{C}_P + \mathcal{C}_Q$. This *faceted Chern number* (\mathcal{C}_f) equals the bulk invariant χ , according to the bulk-boundary correspondence proven in Ref. 33. Crucially \mathcal{C}_f is the net Chern number of the entire Hilbert space $\mathcal{H}_{1/2}[b_{\max}]$ for b_{\max} that is sufficiently large (in the sense described above). The relation $\chi = \mathcal{C}_f \neq 0$ thus implies there exists no exponentially-localized Wannier representation of $\mathcal{H}_{1/2}[b_{\max}]$, for any large b_{\max} ; in particular, this means that no such representation exists as we take $b_{\max} \rightarrow \infty$ in the above-described direct-limit procedure.

2. Delicacy of obstruction principle

When a unicellular, bulk conduction band is added to the Hopf insulator, the Wannier obstruction described in the previous subsection no longer holds for all values of the truncation parameter b_{\max} . Instead, the existence of an obstruction depends on the parity of b_{\max} ; for one parity, we find that the obstruction is removable.

The addition of a unicellular bulk conduction band implies there are two bulk-like, unfilled Bloch-Wannier bands in any interval $[z, z + 1]$, for z that is sufficiently far from the surface termination. The net Chern number of both bulk-like bands vanishes, in accordance with the triviality of the first Chern class in the bulk. However, the two bulk-like bands can have cancelling Chern numbers; by a continuous deformation of Q , it is always possible that one bulk-like band has Chern number $-\mathcal{C}_f$ and the other has Chern number $+\mathcal{C}_f$. In defining the unfilled Hilbert space $\mathcal{H}_Q[b_{\max}]$, we see that advancing b_{\max} by one changes the net Chern number of \mathcal{H}_Q by $\pm\mathcal{C}_f$. Thus there exists b_{\max} of one parity such that the bulk-like Bloch-Wannier bands have a net Chern number $-\mathcal{C}_f$ that cancels the Chern number of the topologically-nontrivial surface bands – this implies that $\mathcal{H}_{1/2}[b_{\max}]$ has trivial Chern number and possesses an exponentially-localized Wannier representation. Note for b_{\max} of the opposite parity that $\mathcal{H}_{1/2}[b_{\max}]$ remains topologically nontrivial.

D. DECOMPOSITION OF SURFACE BANDS OF THE $P3$ -SYMMETRIC MODEL INTO BAND REPRESENTATIONS

Assuming that angular momentum $\ell = 1$ corresponds to point-group representation 2E (and also to little-group representations Γ_3, K_3, K'_2), while $\ell = 2$ corresponds to 1E (and to Γ_2, K_2, K'_3), we find using the BANDREP tool on the Bilbao crystallographic server [44] the following decompositions for the surface bands of the three-band surface models discussed in the main text.

First, $SB_1 \oplus SB_2^a$ is obstructed, meaning it is not decomposable into elementary band representations. That this obstruction is fragile can be proven by adding s orbitals on $1b$ and $1c$ Wyckoff positions as

$$SB_1 \oplus SB_2^a \oplus [A_1 \uparrow G]_{1b} \oplus [A_1 \uparrow G]_{1c} = [(2A_1 \oplus {}^1E \oplus {}^2E) \uparrow G]_{1a}. \quad (S18)$$

In contrast, combinations $SB_1 \oplus SB_2^b$ and $SB_1 \oplus SB_2^c$ are decomposable into elementary band representations, but neither combination satisfies the uniaxial symmetry condition with both Wannier centers on the $1a$ position. In the former case, one of the two Wannier centers lies on the $1c$, while in the latter case it is $1b$:

$$SB_1 \oplus SB_2^b = [A_1 \uparrow G]_{1a} \oplus [{}^2E \uparrow G]_{1c} \quad (S19a)$$

$$SB_1 \oplus SB_2^c = [A_1 \uparrow G]_{1a} \oplus [{}^2E \uparrow G]_{1b}. \quad (S19b)$$

Similar to the decomposition of $SB_1 \oplus SB_2^a$ in Eq. (S18), the direct sums in Eqs. (S20) can be composed with elementary band representations corresponding to Wyckoff positions $1b$ or $1c$, such that the resulting bands are Wannier-representable with orbitals residing solely on the $1a$ Wyckoff position, namely:

$$SB_1 \oplus SB_2^b \oplus [(A_1 \oplus {}^1E) \uparrow G]_{1c} = [(2A_1 \oplus {}^1E \oplus {}^2E) \uparrow G]_{1a} \quad (S20a)$$

$$SB_1 \oplus SB_2^c \oplus [(A_1 \oplus {}^1E) \uparrow G]_{1b} = [(2A_1 \oplus {}^1E \oplus {}^2E) \uparrow G]_{1a}. \quad (S20b)$$

E. FINITE SLAB MODELS

1. Hamiltonian for a slab geometry

Here we present a finite slab Hamiltonian which was used to obtain the spectrum in Fig. 2(a,b). The system is periodic in x and y spatial directions, and open in the z direction with N layers. For sufficiently large N , the surface states of a finite slab (localized to one of the two surface facets) approximates the surface states of a half-infinite slab; the half-infinite geometry plays an important role in the bulk-boundary correspondence discussed in the main text.

The Hamiltonian is represented by an $N \times N$ block matrix that retains its dependence on momentum components k_x and k_y :

$$H_{\text{slab}}^r(k_x, k_y) = \begin{pmatrix} \varepsilon^r & J_1^r & J_2^r & 0 & \dots \\ J_1^{r,\dagger} & \varepsilon^r & J_1^r & J_2^r & \\ J_2^{r,\dagger} & J_1^{r,\dagger} & \varepsilon^r & J_1^r & \\ 0 & J_2^{r,\dagger} & J_1^{r,\dagger} & \varepsilon^r & \\ \vdots & & & & \ddots \end{pmatrix}, \quad (S21)$$

where $\varepsilon^r = \varepsilon^r(k_x, k_y)$ and $J_i^r = J_i^r(k_x, k_y)$ are $r \times r$ blocks of a finite model corresponding to a rank- r bulk Hamiltonian. The block ε^r describes intra-layer potential while J_1^r (J_2^r) describes nearest (next-nearest) neighbor layers coupling. For a minimal

	P_t^r	P_b^r
α_N^2	0	20
α_{N-2}^2	-9	-3
α_N^3	0	20
α_{N-3}^3	-15	-5

Table S1. Coefficients in front of the projectors $P_{t/b}^r P_n P_{t/b}^r$ added to the Hamiltonian to project surface states to the bulk

two-band model (1) of the main text they are given by the following matrices:

$$\varepsilon^2(k_x, k_y) = \begin{pmatrix} |f_{-1}(k_x, k_y)|^2 - [f_0(k_x, k_y) + m]^2 - 17/2 & -i[f_0(k_x, k_y) + m] \cdot f_{-1}(k_x, k_y) \\ i[f_0(k_x, k_y) + m] \cdot f_{-1}^*(k_x, k_y) & -|f_{-1}(k_x, k_y)|^2 + [f_0(k_x, k_y) + m]^2 + 17/2 \end{pmatrix}, \quad (\text{S22a})$$

$$J_1^2(k_x, k_y) = \begin{pmatrix} -4[f_0(k_x, k_y) + m] & -5i/2 \cdot f_{-1}(k_x, k_y) \\ 3i/2 \cdot f_{-1}^*(k_x, k_y) & 4[f_0(k_x, k_y) + m] \end{pmatrix}, \quad (\text{S22b})$$

$$J_2^2(k_x, k_y) = \begin{pmatrix} -15/4 & 0 \\ 0 & 15/4 \end{pmatrix}, \quad (\text{S22c})$$

with $f_i(k_x, k_y)$ given in Eq. (S3c). For a rank-three bulk model with additional valence band with angular momentum $\ell'_v = 2$ the blocks are given by:

$$\varepsilon^3(k_x, k_y) = \left(\begin{array}{c|cc} -50 & 0.4f_2(k_x, k_y) & 0.56f_1(k_x, k_y) \\ \hline 0.4f_2^*(k_x, k_y) & & \\ 0.56f_1^*(k_x, k_y) & & \end{array} \middle| \begin{array}{c} \varepsilon^2(k_x, k_y) \end{array} \right), \quad (\text{S23a})$$

$$J_1^3(k_x, k_y) = \left(\begin{array}{c|cc} 0 & 0.8f_2(k_x, k_y) & 0.8f_1(k_x, k_y) \\ \hline -0.24f_2^*(k_x, k_y) & & \\ 0.32f_1^*(k_x, k_y) & & \end{array} \middle| \begin{array}{c} J_1^2(k_x, k_y) \end{array} \right), \quad (\text{S23b})$$

$$J_2^3(k_x, k_y) = \left(\begin{array}{c|cc} 0 & 0 & 0 \\ \hline 0 & & \\ 0 & & \end{array} \middle| \begin{array}{c} J_2^2(k_x, k_y) \end{array} \right). \quad (\text{S23c})$$

The spectra in Fig. 2(a, b) are calculated for the given two- and three-band system, respectively, with $N = 50$ layer thickness and parameter value $m = -6$.

2. Algorithm to detach a surface state

Here we describe the algorithm which was used to detach surface bands from the rest of the spectrum in the slab models described in Sec. E 1. Importantly, we modify Hamiltonian only on the surface thus keeping the bulk unaffected.

First, describe the detachment procedure in a two-band model. Since we are interested in only one (lower) surface we completely remove the upper surface state from the gap by adding a potential expressed by a diagonal matrix $V = \text{diag}(17, 3)$ to the corresponding intra-layer block $H_{\text{slab};NN}^2 \rightarrow H_{\text{slab};NN}^2 + V$. To detach the lower surface band we reduce the lower-most intra-layer potential by multiplying it with 0.3 factor and add a potential $V = I$, with I being identity matrix: $H_{\text{slab};11}^2 \rightarrow 0.3H_{\text{slab};11}^2 + I$. Effectively, this brings the lower surface state closer to zero energy and detaches it from the bulk bands.

The same steps with slightly different parameters made for a three-band model allow to detach two surface bands from the rest of the spectrum. Thus, upper surface state is removed by $H_{\text{slab};NN}^3 \rightarrow H_{\text{slab};NN}^3 + \text{diag}(3, 17, 3)$ while two lower surface states are detached by $H_{\text{slab};11}^3 \rightarrow 0.3H_{\text{slab};11}^3 + \text{diag}(42, 0, 0)$.

While not essential to the detaching procedure, in deriving Fig. 2(a,b) we performed an additional step of pushing all hybrid bands (which are partially surface-like and partially bulk-like) out of the bulk energy gap. This ‘pushing’ is done by the method of projectors: at each point in the rBZ (k_x, k_y) for the n^{th} eigenvector $|u_n\rangle$ (its eigenenergy is on the n -th place in the increasing order) we define a projector $P_n = |u_n\rangle\langle u_n|$. Additionally define a projector to the top (bottom) layer $P_{t/b}^r$ which has all elements zero except the last (first) $r \times r$ diagonal block which is the identity matrix. Modification of the Hamiltonian $H_{\text{slab}}^r \rightarrow H_{\text{slab}}^r + \alpha_n^r P_{t/b}^r P_n P_{t/b}^r$ with a properly chosen real coefficient α_n^r allows to project the surface-localized part of the n -th eigenstate to the bulk spectrum which effectively removes the corresponding energies from the gap. Fig. 2(a,b) is obtained after performing a series of projections with non-zero coefficients presented in Tab. S1 first for a two-band and then for a three-band model.